Drone Detection with Chirp-Pulse Radar Based on Target Fluctuation Models

Byung-Kwan Kim, Junhyeong Park, Seong-Jin Park, Tae-Wan Kim, Dae-Hwan Jung, Do-Hoon Kim, Taihyung Kim, and Seong-Ook Park

This paper presents a pulse radar system to detect drones based on a target fluctuation model, specifically the Swerling target model. Because drones are small atypical objects and are mainly composed of non-conducting materials, their radar cross-section value is low and fluctuating. Therefore, determining the target fluctuation model and applying a proper integration method are important. The proposed system is herein experimentally verified and the results are discussed. A prototype design of the pulse radar system is based on radar equations. It adopts three different pulse modes and a coherent pulse integration to ensure a high signal-to-noise ratio. Outdoor measurements are performed with a prototype radar system to detect Doppler frequencies from both the drone frame and blades. The results indicate that the drone frame and blades are detected within an instrumental maximum range. Additionally, the results show that the drone's frame and blades are close to the Swerling 3 and 4 target models, respectively. By the analysis of the Swerling target models, proper integration methods for detecting drones are verified and can thus contribute to increasing in detectability.

Keywords: Doppler measurements, Doppler radar, Millimeter wave radar, Radar signal processing.

I. Introduction

Detecting small targets that have a low radar cross-section (RCS) by using radar is a challenging task [1], [2]. Drones, also known as unmanned aerial vehicles, are increasingly being used for many purposes, such as surveillance, logistics, and aerial recordings, because they are much less expensive and easier to operate than conventional aircraft. Drones are difficult to detect with a radar system since their frames and blades are comprised of non-conducting materials, which lead to much smaller RCS values compared to conventional flight vehicles. In addition, they fly slower at lower altitudes than other flying objects; therefore, it is challenging to distinguish them from typical radar clutters. Considering typical radar clutters and the RCS of potential targets, the rotating blades of a drone lie in the clutter-free region since they have a high radial velocity with a very low RCS. Thus, to detect and identify drones, it is more effective to detect the Doppler frequencies produced by not only the drone's movement, but also the drone's rotating blades.

To detect drones with a low RCS, various radar systems for detecting drone movement have been recently proposed [3], [4]. However, it is difficult to recognize the drones from only the Doppler frequency caused by the movement of the drone body. This is because it does not determine the features of the drone itself. In terms of blades of aircraft and drones, previous radar studies focused on the characteristic of a returned radar signal to distinguish targets by analyzing the characteristic. Early studies [5]–[7] concluded that the returned radar signal from a rotating object is amplitude- and frequency-

Manuscript received Mar. 26, 2017; revised Aug. 3, 2017; accepted Nov. 30, 2017.

Byung-Kwan Kim (seid@kaist.ac.kr), Junhyeong Park (bdsfh0820@kaist.ac.kr), Seong-Jin Park (corresponding author, pondsky@kaist.ac.kr), Tae-Wan Kim (gold427@kaist.ac.kr), Dae-Hwan Jung (daeman88@kaist.ac.kr), Do-Hoon Kim (dohoonh@kaist.ac.kr), and Seong-Ook Park (soparky@kaist.ac.kr) are with the Microwave and Antenna Laboratory, School of Electrical Engineering, Korea Advanced Institute of Science and Technology, Daejeon, Rep. of Korea.

Taihyung Kim (stnc@stnc.co.kr) is with System Technology & Control, Daejeon, Rep. of Korea.

modulated by approaching quasi-stationary methods. A recent study [8] showed that these signals can be analyzed in a time-frequency plot, namely a micro-Doppler signature or a spectrogram. Additionally, a study based on the micro-Doppler signature [9]–[15] produced an efficient method based on the micro-Doppler signature to distinguish and classify targets.

Although micro-Doppler signature analysis is effective at distinguishing targets from other clutters, the detection itself of drone blades is challenging because the drone blades are much smaller than the body; moreover, the RCS changes from moment to moment. To solve this problem, applying pulse integration to address adequate gain and determining the requisite specifications of drone detection radar should be conducted, followed by micro-Doppler analysis for accurate detection.

Previous studies have been limited to detecting drone movement or the micro-Doppler of its blades. However, in our study, we consider the target fluctuation model of both the drone body and blades. The target fluctuation model was first presented by Swerling [16], who showed that the radar targets can be classified by the RCS fluctuation due to their movement or rotation. In addition, detection probability of the targets was derived with the chi-square model. If we apply a proper integration method according to the Swerling model of the drone, the detectability can be significantly increased. In this study, we thus measured the returned signals from the drone's vertically and horizontally rotating blades using commercial chirp-pulse radar. We estimated the target fluctuation model of the drones based on the measurement results. Accordingly, we propose a proper integration method.

The remainder of this paper is organized as follows. In Section II, the prototype pulse radar system is described. In Section III, the experiment setup and results are presented and discussed. In Section IV, the study conclusions are presented.

II. Chirp-Pulse Doppler Radar Prototype

The radar prototype is depicted in Fig. 1; the specifications are listed in Table 1. The prototype is a chirp-pulse Doppler monostatic radar, which uses a 34.5 GHz carrier frequency. We introduce three distinct pulse modes to overcome an ambiguity problem and the large minimum range of pulse compression radar. The developed system transmits and receives three types of pulses in one pulse repetition frequency (PRF).

The pulse Doppler radar detects the distance of a target by the time difference between the transmitted signal and the received signal. As the pulse width increases, the pulse gives a higher average power in transmitting. Therefore, longer pulses are more advantageous for detecting long distances [17]. However, the range resolution is degraded and the minimum detectable range increases as the pulse width increases [17].

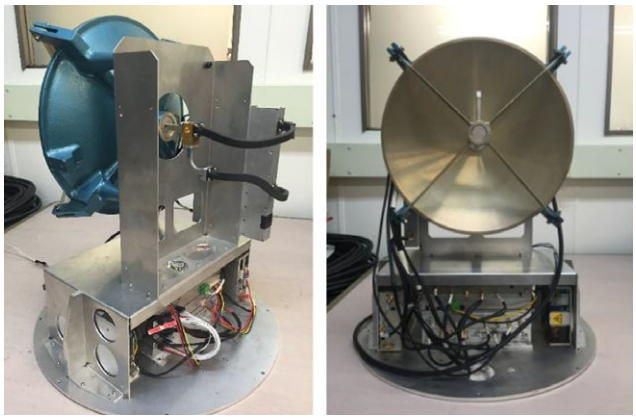

Fig. 1. Prototype Doppler radar system.

Table 1. Prototype radar specifications.

Item	Specification
Detection range	1 km
Range resolution	2.02 m
Center frequency	34.5 GHz
Antenna	Reflector antenna
Peak power	0.2 W
Receiver noise floor	6 dB
Pulse width	20 ns, 1 μs, 4 μs
Pulse repetition frequency	23.08095 kHz

To overcome the trade-off between the long-range detection and range resolution, we modulate a linear chirp with a 60 MHz bandwidth in the medium and long pulses, and the pulse compression technique is applied. Accordingly, the range resolution can be improved, even with the long pulse [17]. In addition, we reduce the minimum detectable range by using medium and short pulses. Thus, we can fully cover the range from 0 km to 1 km. Moreover, the transmitting and receiving time frame is designed to detect the target within 225 m with a short pulse, 227 m to 675 m with a medium pulse, and 677 m to 1,001 m with a long pulse, as shown in Fig. 2. By making the intervals between pulses different, the ambiguity problem can be resolved [18]. Furthermore, the offset timings are introduced at the receiver to attenuate the strong signals from ground clutters. This is called sensitivity time control (STC).

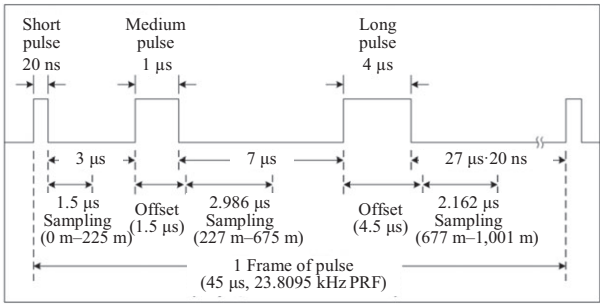

Fig. 2. Pulse timing diagram of proposed system (not to scale).

With the described time frame, the radar equation is used to derive the maximum detectable RCS within a given range. The equation can be expressed as

$$R^4 = \frac{n \cdot P_t \cdot G_t \cdot G_r \cdot \sigma \cdot \lambda^2}{(4\pi)^3 K \cdot T_0 \cdot B \cdot F_n \cdot \left(\frac{S_0}{N_0}\right) \cdot L_x} = \frac{P_{av} \cdot t_f \cdot G_t \cdot G_r \cdot \sigma \cdot \lambda^2}{(4\pi)^3 K \cdot T_s \cdot D(n) \cdot L_x}, \quad (1)$$

where $D(n)$ is a detectability factor with the number of pulse integrations as n [16], σ is the RCS, and G denotes the antenna gain (transmitter/receiver). In addition, λ is the wavelength at the carrier frequency, K is the Boltzmann's constant, T_0 represents the absolute temperature in Kelvin, P_{av} denotes the average power, and T_s is the system temperature. The antenna return loss (1 dB), processing loss (2 dB), beam shape loss (1 dB), and radio frequency (RF) transmission loss between components (1.5 dB) are assumed and summed up as L_x [16].

The output power of the transmitter for P_{av} and the noise figure of the receiver for T_s are needed to solve the above equation. The transmit power is 0.2 W and the noise floor is 6 dB. These values are obtained by the performance measurement of the transmit–receive module used for the proposed radar system. The average power, P_{av}, is the product of the transmit power, pulse length, and PRF. Moreover, t_f is the product of the coherent detection number and pulse repetition interval (PRI). In terms of the number of integrations (n), the maximum detectable range increases as n increases. However, the processing time will limit n. A large n requires a long processing time. We should optimize n by testing digital processors because the processing time depends on the performance of the digital processors. With the digital processors in the radar system, we concluded that the optimum n is 64. Thus, the prototype radar adopts the pulse integration with 64 coherent pulses. With the 64 coherent pulse integration, the detectability factor $D(64)$ is referred to as 0.8 dB; when the target has no fluctuation loss (Swerling case 0), the detection probability is 0.9, and the false-alarm number is 6×10^5 [16]. Since the designed radar system is monostatic, the antenna gain remains the same.

To summarize, the gain and loss parameters for the short pulse are presented in Table. 2. Using (1), we adjust the width of the pulses to sufficiently cover the intended maximum detectable ranges of each pulse. The known RCS of the frame of a micro-drone, -25 dBm^2, is assumed. Finally, we decide that 20 ns, 1 μs, and 4 μs are the short, medium, and long pulse widths. The average powers for the short ($P_{av,s}$), medium ($P_{av,m}$) and long pulse ($P_{av,l}$), respectively, are

$$P_{av,s} = P_t \cdot \tau_s \cdot f_{PRF} = 200 \times 10^{-3} \times 20 \times 10^{-9} \times \frac{10^6}{42} = -40.21\,(\text{dBW}), \quad (2)$$

$$P_{av,m} = P_t \cdot \tau_m \cdot f_{PRF} = 200 \times 10^{-3} \times 10^{-6} \times \frac{10^6}{42} = -23.22\,(\text{dBW}), \quad (3)$$

$$P_{av,l} = P_t \cdot \tau_l \cdot f_{PRF} = 200 \times 10^{-3} \times 4 \times 10^{-6} \times \frac{10^6}{42} = -17.2\,(\text{dBW}). \quad (4)$$

Thus, the maximum detectable ranges for each pulse can be calculated as 283.69 m, 754.36 m, and 1,066.83 m by (1). It can be concluded that these values are adequate to cover the intended maximum detectable ranges of each pulse. Additionally, as the calculated maximum detectable range exceeds the aimed maximum detectable range, the

Table 2. Gain and loss parameters of the short pulse for maximum detectable RCS with the given range of 225 m.

Parameters	P_{av}	t_f	G	σ	λ	T_s	$D(64)$	L_x	Constants	SUM
dB (+)	N/A	N/A	36	N/A	N/A	N/A	N/A	N/A	75.625	147.625
dB (−)	40.212	25.7057	N/A	?	41.214	31.08	0.8	5.5	N/A	?

https://doi.org/10.4218/etrij.2017-0090

maximum detectable RCS for the short pulse (σ_{s_max}) can be obtained by substituting the calculated maximum detectable range and the other parameters in Table 2 for (1) as -29.03 dBm^2.

Similarly, for the medium and long pulses, the maximum detectable RCS can be calculated as -26.93 dBm^2 and -26.11 dBm^2. Considering that the known RCS of a bird is -20, that of a human is 0, and the frame of a micro-drone is -25 dBm^2, it can be predicted that the radar with the proposed performance can detect micro-drones.

III. Experiment Setup and Results

Measurements were obtained at a straight section of a riverside road in Daejeon, Rep. of Korea. As depicted in Fig. 3, the pulse Doppler radar was operated with a control PC and power supply. Measurement A (flying drone) and measurement B (fixed drone) were then obtained. The measurements were performed only when there was no detected target with a constant false-alarm rate detector.

The objective of measurement A was to detect the movement of the drone's frame; that of measurement B was to identify the drone with the Doppler frequencies from the horizontal/vertical rotation of the blades. The blades used for this experiment did not rotate vertically. However, the whole drone was vertically inclined up to 90 degrees to determine if the system could detect the Doppler from a drone with vertically rotating blades (such as the MQ-1 Predator from General Atomics). To compare the detectability for each case, we counted the number of detections in different situations for 60 s.

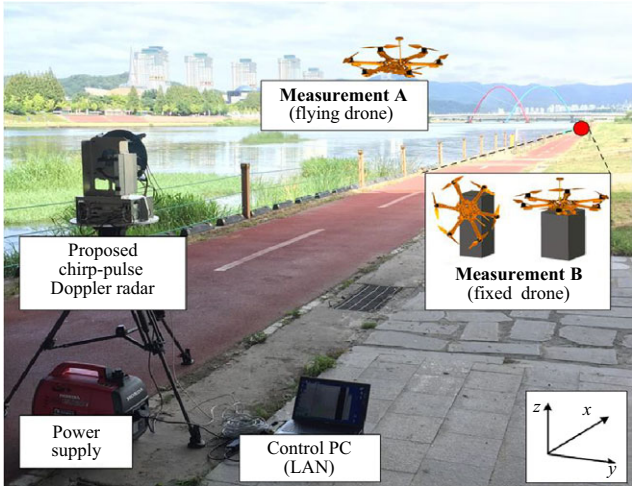

Fig. 3. Measurement setup for detecting a flying (measurement A) and fixed (measurement B) drone beside a river.

The unmanned drone used in this experiment was a Bumblebee F820 hexacopter from Hobbylord Corporation. The drone height was 440 mm and the diameter was 820 mm. All six motors (XM5010TE-9MR; 360 rpm/V; DualSky Corporation) rotated both clockwise and counterclockwise and were controlled by the Naza-M multi-rotor controller [19]. The drone had six attached carbon-fiber propellers called MRP-15 and made by DualSky Corporation [20] (Fig. 4). Two types of blades were employed for each rotation direction and they were symmetric to each other.

Firstly, the flying drone was measured. The drone was set to fly in a straight line with a constant speed (4.67 m/s). Figure 5 presents the measured distance of the drone from the radar system and the calculated distance using the known speed of the drone. The drone departed at a 550 m position; however, owing to the initial stability of the drone flight, the measurement was started from 559 m. The initial position was measured with a walking distance measurement device. As depicted in Fig. 5, the implemented radar continuously detected the drone's flight, and the number of detections in 1 min was 484. There were

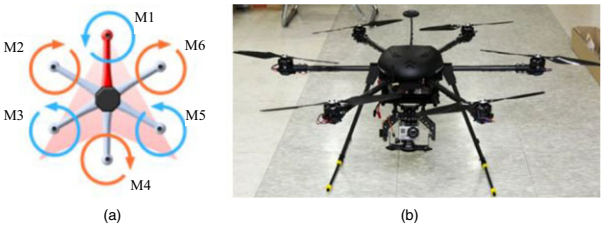

Fig. 4. Hexacopter (a) rotation direction [20] and (b) image.

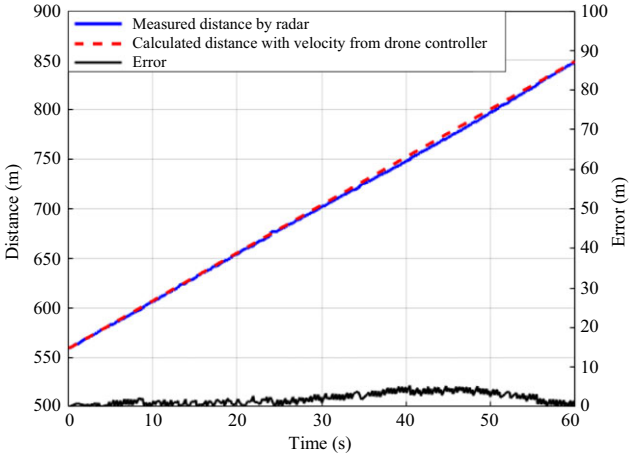

Fig. 5. Result of measurement A. The drone's distance is measured by the proposed radar, and the distance calculated by the velocity from the drone controller is presented for comparison. Errors are also shown.

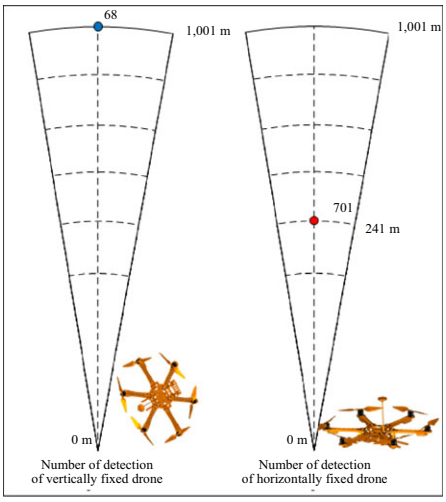

Fig. 6. Result of measurement B: number of detections at the maximum detection range.

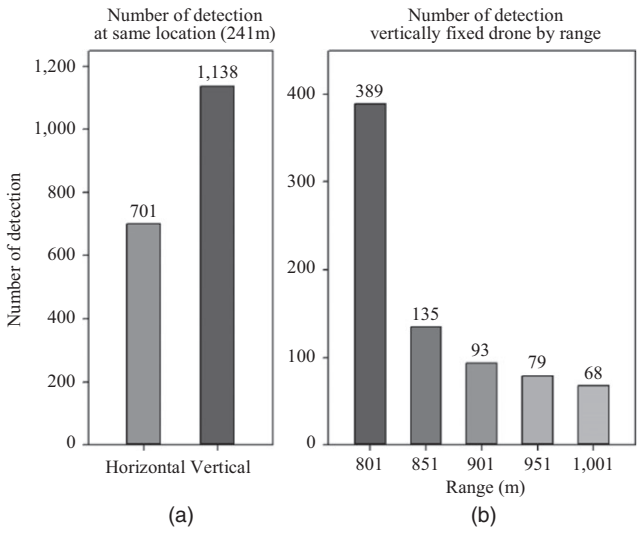

Fig. 7. Result of measurement B: number of detections of (a) the vertically and horizontally fixed drone at the same location, and (b) the vertically fixed drone at a different range.

small errors between the calculated and measured distance because the flight was slightly affected by wind.

After flight measurement A, fixed drone measurement B was performed to determine the detectability of the drone's rotating blades using our radar system. The drone was measured every 50 m from the maximum detectable range (1,001 m) to the closest point. The experimental results in Fig. 6 show that the system could detect the vertically rotating blades up to its maximum measurement range (1,001 m), whereas the radar could detect the horizontally rotating blades only up to a certain distance (241 m).

In Fig. 7, the number of detections at the same location by different fixation directions (a) and the number of detections by different ranges (b) are presented. As presented in Fig. 7(a), the number of detections of the horizontally fixed drone is less than those of the vertical one at the same distance. Moreover, the maximum detectable range of the vertically fixed drone is much greater than that of the horizontally fixed one. Since the size and surface area of the target is the major factor that affects RCS, it can be concluded that the RCS values of the vertically and horizontally rotating blades of the drones considerably differ.

As shown by the line of sight of the radar, the surface area of the horizontally rotating blade is approximately 0.003 m^2 for one blade when the blade is at a normal position to the line of sight. On the other hand, the surface area of the vertically rotating blade is 0.07 m^2. Furthermore, the radar cannot simultaneously detect all six blades when the target drone is fixed horizontally because some blades remain concealed by others placed in front of them. However, the radar can detect all six vertically rotating blades because the blades are positioned in the plane normal to the radar sight.

As presented in Fig. 7(b), the number of detections from the rotating vertically fixed drone decreases as the distance increases, which is a natural consequence since the SNR decreases as the distance increases, and the reduced SNR results in fewer detections. The number of detections of the horizontally fixed drone is the largest at the maximum detection range; however, the detection is not available for further distances. The reasons for the shorter detection range and sudden undetectability of the horizontally rotating blades are the following: 1) The RCS value of the blades is small because the surface area of the blades is tiny when they are horizontally rotating. Therefore, the required SNR is higher than that in the vertical case. 2) The RCS of the horizontally rotating blades rapidly fluctuates from pulse to pulse, such as in Swerling model 2 or 4.

Considering that the drone is comprised of a frame and blades, which are large, and a small scatterer, it can be concluded that the drone's frame is the Swerling 3 target and the drone's rotating blades comprise the Swerling 4 target. Note that the blade fluctuation is significantly affected by an aspect angle of the radar.

In the pulse integration theory, the performance of coherent integration is better than non-coherent integration for non-fluctuating targets. However, it has not been preferred in radar developments because it is not cost-effective, and its integration gain vanishes for Swerling 2 and 4 targets [16]. Nevertheless, the coherent integration

https://doi.org/10.4218/etrij.2017-0090

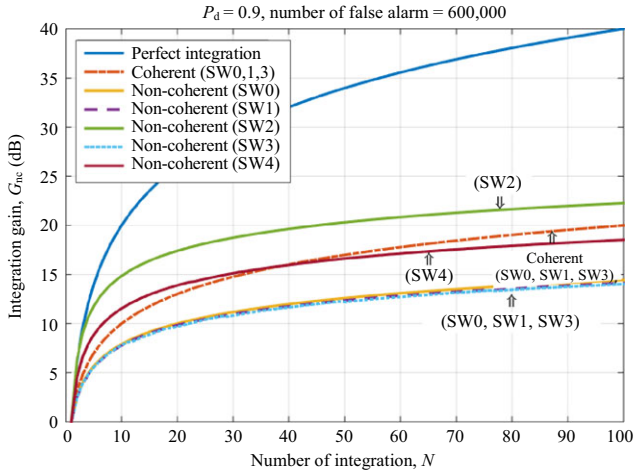

Fig. 8. Integration gain as a function of the number of integrated pulses for different types of target fluctuations based on the probability of detection and the false-alarm number for the prototype radar system.

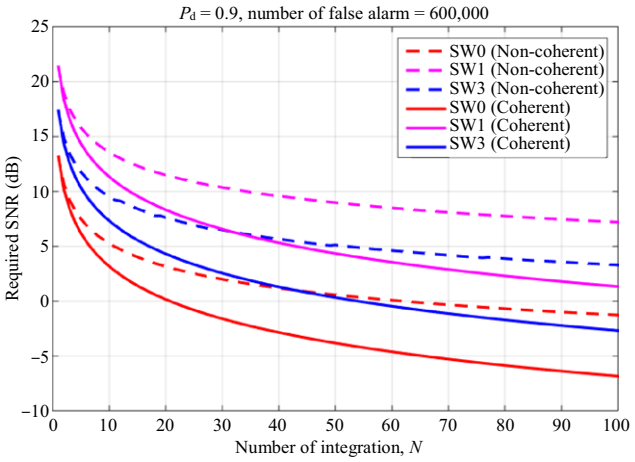

Fig. 9. Comparison of the required SNR versus the number of integrations with given probability of detection P_d and the number of false alarms, N_{fa}.

performs better than non-coherent integration for non-fluctuating targets and Swerling 1 and 3 targets. The integration gain for Swerling targets with coherent/non-coherent integration is calculated for our radar system prototype [16], [17] and presented in Fig. 8. The figure indicates that the integration gains of the Swerling case 0, 1, and 3 are similar, and their differences are within 0.1 dB [2], [21]. However, it does not mean that the required SNR is the same for each case. Using a given probability of detection and the number of false alarms, the required SNR can be calculated and plotted in Fig. 9. The difference of the required SNR between each model is 4.1 dB, and that between integration methods is 4.8 dB for 64 pulse integration, respectively.

From Figs. 8 and 9, it can be concluded that coherent integration is better than non-coherent integration when the target is not fluctuating or is slowly fluctuating from scan to scan (Swerling 1, 3). Since the first objective of our prototype radar is to detect the movement of the drone's frame with low transmitting power, we adopted coherent pulse integration using off-the-shelf digital processors at a low cost. As shown in the results of measurement A, by using coherent integration, we successfully detected the movement of the drone's frame.

With respect to blade detection, coherent integration is useless for this type of target, which rapidly fluctuates from pulse to pulse. In the case of non-coherent integration, the gain of the fluctuating target (Swerling 2, 4) is higher than the non-fluctuating cases, as depicted in Fig. 8. Additionally, the coherent integration provides no gain for these kinds of targets. Therefore, non-coherent integration is a better approach for the detection of the rotating drone's blade to distinguish or identify the target as a drone. Moreover, with respect to blade detection, the aspect angle is a critical factor in determining the blade's detectability because fluctuations of both RCS and RCS itself are dramatically changed by the aspect angle.

From the measurement results and analysis on the integration gain with target models, it can be concluded that the proposed system detected the drone's frame by the gain from coherent pulse integration. However, detection of the rotating blade of the drone was not successful for all cases because the coherent pulse integration did not work for RCS fluctuation from the blade rotation. Through the measurement results and analysis, we found that a valid method for a target can be invalid for different measurement situations.

IV. Conclusion

In this study, the Swerling target model of a drone was estimated using the results from the presented prototype of a chirp-pulse radar. Based on the radar equation, the pulse timing of the prototype radar is designed with three different pulse modes. The low-cost implemented prototype radar employs off-the-shelf digital processors and adopts coherent pulse integration to secure a high SNR to detect targets that have a low RCS.

The results indicated that the realized system detected the movement of the frame of the flying drone and its rotating blades, as well as the stationary drone. The results additionally showed that the detectability of the vertically fixed drone was better than that of the horizontally fixed drone on account of the rapid fluctuation of the blade's RCS.

Based on the results and in accordance with Swerling's theory, the drone frame and blades were estimated from the Swerling 3 and 4 targets, respectively. From the integration gain analysis based on the Swerling target model, it was verified that the coherent integration performed better for non-fluctuating targets and Swerling 1 and 3 targets. On the other hand, for the targets with rapid fluctuation, only non-coherent integration was an effective integration method. Therefore, in terms of drone detection, both coherent and non-coherent integration should be considered since the drones have a low SNR and a rapid fluctuation of RCS.

Acknowledgements

This work was supported by a project of UAV Safety Technology Research called "Flight Safety Regulation Development and Integrated Operation Demonstration for Civil RPAS" (Grant No. 17ATRP-C108186-03), funded by the Ministry of Land, Infrastructure and Transport, government of the Rep. of Korea; and, in part, by the Basic Science Research Program through the National Research Foundation of Korea, funded by the Ministry of Science (Grant No. 2016R1A2B4010918).

References

[1] E.G. Alivizatos, M.N. Petsios, and N.K. Uzunoglu, "Towards a Range-Doppler UHF Multistatic Radar for the Detection of Non-cooperative Targets with Low RCS," *J. Electromagn. Waves Appl.*, vol. 19, no. 15, 2005, pp. 2015–2031.

[2] D.P. Meyer, *Radar Target Detection*, New York, NY, USA: Academic Press, 1973.

[3] J. Drozdowicz et al., "35 GHz FMCW Drone Detection System," *Int. Radar Symp.*, Krakow, Poland, May 10–12, 2016, pp. 1–4.

[4] J. Klare, O. Biallawons, and D. Cerutti-Maori, "Detection of UAVs Using the MIMO Radar Miracle-KA," *Proc. EUSAR 2016: Eur. Conf. Synthetic Aperture Radar*, Hamburg, Germany, June 6–9, 2016, pp. 1–4.

[5] J. Martin and B. Mulgrew, "Analysis of the Effects of Blade Pitch on the Radar Return Signal from Rotating Aircraft Blades," *Int. Conf. Radar*, Oct. 1992, pp. 446–449.

[6] J. Martin and B. Mulgrew, "Analysis of the Theoretical Radar Return Signal from Aircraft Propeller Blades," *Record IEEE 1990 Int. Radar Conf.*, Arlington, VA, USA, May 7–10, 1990, pp. 569–572.

[7] S.Y. Yang, S.M. Yeh, S.S. Bor, S.R. Huang, and C.C. Hwang, "Electromagnetic Backscattering from Aircraft Propeller Blades," *IEEE Trans. Magn.*, vol. 33, no. 2, Mar. 1997, pp. 1432–1435.

[8] V.C. Chen, *The Micro-Doppler Effect in Radar*, Norwood, MA, USA: Artech House, 2011.

[9] F. Fioranelli, M. Ritchie, and H. Griffiths, "Classification of Unarmed/Armed Personnel Using the NetRAD Multistatic Radar for Micro-Doppler and Singular Value Decomposition Features," *IEEE Geosci. Remote Sensing Lett.*, vol. 12, no. 9, Sept. 2015, pp. 1933–1937.

[10] Y. Kim and T. Moon, "Human Detection and Activity Classification Based on Micro-Doppler Signatures Using Deep Convolutional Neural Networks," *IEEE Geosci. Remote Sensing Lett.*, vol. 13, no. 1, Jan. 2016, pp. 8–12.

[11] G.J. Mendis, T. Randeny, J. Wei, and A. Madanayake, "Deep Learning Based Doppler Radar for Micro UAS Detection and Classification," *IEEE Military Commun. Conf.*, Baltimore, MD, USA, Nov. 1–3, 2016, pp. 924–929.

[12] M. Ritchie, F. Fioranelli, H. Griffiths, and B. Torvik, "Monostatic and Bistatic Radar Measurements of Birds and Micro-Drone," *IEEE Radar Conf.*, Philadelphia, PA, USA, 2016, pp. 1–5.

[13] M. Ritchie, F. Fioranelli, H. Borrion, and H. Griffiths, "Multistatic Micro-Doppler Radar Feature Extraction for Classification of Unloaded/Loaded Micro-Drones," *IET Radar Sonar. Navig.*, vol. 11, no. 1, 2017, pp. 116–124.

[14] M. Jahangir, C.J. Baker, and G.A. Oswald, "Doppler Characteristics of Micro-Drones with L-Band Multibeam Staring Radar," *IEEE Radar Conf.*, Seattle, WA, USA, 2017, pp. 1052–1057.

[15] B. Cagliyan and S.Z. Gürbüz, "Micro-Doppler-Based Human Activity Classification Using the Mote-Scale BumbleBee Radar," *IEEE Geosci. Remote Sensing Lett.*, vol. 12, no. 10, Oct. 2015, pp. 2135–2139.

[16] P. Swerling, "Probability of Detection for Fluctuating Targets," *ASTIA Document Number AD 80638*, Mar. 17, 1954.

[17] M. Skolnik, *Radar Handbook*, 2nd ed., Boston, MA, USA: McGraw-Hill, 1990.

[18] T.K. Sarkar and J. Koh, *Coherent Processing across Multiple Staggered Pulse Repetition Interval (PRI) Dwells in Radar*, Syracuse, NY, USA: Syracuse Univ., Feb. 2004.

[19] NAZA-M V2 Product, DJI Inc., Shenzhen, China. http://www.dji.com/product/naza-m-v2

[20] MRP-15 Carbon Fiber Propeller Product, DualSky Inc., Shanghai, China. http://www.dualsky.com/wiring_plugs/mr_propeller.shtml

[21] M.A. Richards, *Fundamentals of Radar Signal Processing*, NY, USA: McGraw-Hill, 2005.

Byung-Kwan Kim received his BS degree in information and communication engineering from Korea Advanced Institute of Science and Technology (KAIST), Daejeon, Rep. of Korea, in 2010, and MS (2012) and PhD (2017) degrees in electrical engineering from KAIST. His current research interests are pulsed radar, antenna numerical analysis, and antenna design.

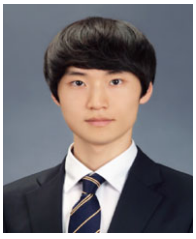

Junhyeong Park received his BS and MS degrees in electrical engineering from Korea Advanced Institute of Science and Technology (KAIST), Daejeon, Rep. of Korea, in 2015 and 2017, respectively. He is currently pursuing the PhD degree in electrical engineering at KAIST. His current research interests include frequency-modulated continuous-wave radar systems for drone detection, continuous-wave Doppler radar for biomedical applications, and radar signal processing.

Seong-Jin Park received his BS degree in electronic engineering from Korea Aerospace University, Goyang, Rep. of Korea, in 2014. He is currently pursuing an integrated MS and PhD degrees in electrical engineering at Korea Advanced Institute of Science and Technology, Daejeon, Rep. of Korea. His current research interests include design of mm-wave antennas, radar systems, and channel measurement.

Tae-Wan Kim received his BS degree in electrical engineering from Konkuk University, Seoul, Rep. of Korea, in 2013, and his MS degree from Korea Advanced Institute of Science and Technology (KAIST), Daejeon, Rep. of Korea, in 2015. He is currently pursuing a PhD degree in electrical engineering at KAIST. His current research interests are ferrite-loaded antennas and material measurement.

Dae-Hwan Jung received his BS degree in electronic and electrical engineering from Sungkyunkwan University, Suwon, Rep. of Korea, in 2014, and his MS degree in electrical engineering from Korea Advanced Institute of Science and Technology (KAIST), Daejeon, Rep. of Korea, in 2016. He is currently pursuing his PhD degree in electrical engineering at KAIST. His current research interests are frequency-modulated continuous wave (FMCW) design of radar systems and radar signal processing.

Do-Hoon Kim received his BS degree in electrical and electronic engineering from Yonsei University, Seoul, Rep. of Korea, in 2017. He is currently pursuing his MS degree in electrical engineering at Korea Advanced Institute of Science and Technology, Daejeon, Rep. of Korea. His current research interest is radar signal processing.

Taihyung Kim received his BS degree from Chonnam National University, Gwangju, Rep. of Korea in 1979, and MS and PhD degrees from Korea Advanced Institute of Science and Technology, Daejeon, Rep. of Korea in 1981 and 2001, respectively, all in electrical engineering. From April 1981 to May 1996, he was a research engineer at the Korea Agency for Defense and Development, Daejeon, Rep. of Korea in radar and communication systems. Since May 2005, he has been the chief executive officer of the company, System Technology and Control (ST&C), in the Rep. of Korea. His interests are radar signal processing, digital modems, and servo control systems.

Seong-Ook Park received his BS degree from Kyungpook National University, Daegu Rep. of Korea, in 1987; his MS degree from Korea Advanced Institute of Science and Technology (KAIST), Daejeon, Rep. of Korea, in 1989; and his PhD degree from Arizona State University, Tempe, USA, in 1997, all in electrical engineering. From March 1989 to August 1993, he was a research engineer of microwave systems and networks at Korea Telecom, Daejeon, Rep. of Korea. He later joined the Telecommunication Research Center, Arizona State University, until September 1997. Since October 1997, he has been a professor at KAIST. His research interests include antennas, radar systems, and analytical and numerical techniques in electromagnetics. He is a member of Phi Kappa Phi.

https://doi.org/10.4218/etrij.2017-0090